Bulletin of the Mineral Research and Exploration

http://bulletin.mta.gov.tr

Geothermal gradient variation in the Büyük Menderes Graben: implications for geothermal potential of the graben, Western Anatolia, Türkiye

Adrian WIGGINS[a]* and İbrahim ÇEMEN[a]

[a]University of Alabama, Department of Geological Sciences, Tuscaloosa, USA.

Research Article

ABSTRACT

The Büyük Menderes Graben (BMG) is an E-W oriented active extensional geothermal basin within the Menderes Massif, a metamorphic core complex, in Western Anatolia, Turkey. 1500 (megawatts-energy) MWe of installed geothermal capacity for power production exist as of December 2019 in Western Anatolia, mostly generated in the BMG. While the BMG is a vastly producing geothermal resource, it is predicted that it has higher production potential. This study aims to a) quantitatively test the geothermal gradients in the Aydın-İncirliova-Osmanbükü Geothermal Field (IGF), and b) compare the IGF with a neighboring geothermal field. This study also aims to compare the IGF with a neighboring geothermal field. To complete this study, information from stratigraphic columns, bottom hole temperatures, and continuous temperature logs from 13 geothermal wells is utilized with Leapfrog Geothermal to create 3D models of the geology and subsurface temperature distribution. Then, isothermal contour maps of the field are created. The geologic modeling suggests that synextensional deposition has occurred within the graben. The temperature modeling suggests both that thermal breakthrough may have occurred in the field, and that the IGF has a higher geothermal gradient than the nearby Germencik Geothermal Field.

1. Introduction

The Büyük Menderes Graben (BMG) is an E-W oriented active extensional basin within the Menderes Massif, a metamorphic core complex, in Western Anatolia, Turkey. It is part of a graben system that includes the BMG and three smaller N-S oriented grabens, comprising nearly 2200 km² and extending about 140 km from the Aegean Sea in the west to the Denizli Graben (Figure 1) in the east (Özpolat et al., 2020). The three N-S oriented grabens are the Cine, Bozdoğan and Karacasu Grabens (Figure 1).

The BMG is a geothermal basin in the Western Anatolia Geothermal Province (Özgür and Çalışkan,

2013; Yamanlar et al., 2020). In total, 1500 (megawatts-energy) MWe of installed geothermal capacity for power production exist as of December 2019 in Western Anatolia, most of which is generated in the BMG (Yamanlar et al., 2020) from many geothermal power plants, from east to the west, Kızıldere, Pamukören, Salavatlı, Hüseyinciler, Yılmazköy and Germencik (Figure 2).

Faulds et al. (2010) proposed that the geothermal resources of the BMG are inherently linked to geodynamic and structural controls. For example, crustal-scale geoelectrical evidence suggests that extensional tectonics control the flow of geothermal

fluids utilizing both high and low-angle normal faults. Faulds et al. (2010) suggested that elevated heat flow results from fault termination splays, or horsetails, in the western section of the BMG. Alemdar (2015) suggested that asthenospheric material has risen beneath the eastern section of the BMG, which may be a regional source of heat (Figure 6). Yamanlar et al. (2020) noted that the geothermal gradient is variable throughout the BMG, with the highest gradient in the eastern section and the lowest in the middle of the graben (Figure 3). Tonkul et al. (2021) performed 3D reservoir temperature modeling of the Germencik Geothermal Field (GGF) in the western BMG, showing reservoir temperatures vary between 150-200°C. The reservoir temperatures for the middle of the graben have been reported to be between 169 °C–188 °C (Haklıdır and Şengün, 2020). However, the reason

why the geothermal gradient differs so drastically throughout this region it not well understood.

This study will test the hypothesis that rising asthenospheric material and fault splays may contribute to the E-W geothermal gradient variability in the BMG. The models show the areas of high geothermal gradient, which indicate the areas with high geothermal potential. We will interpret the models based on geological and geophysical data to determine if there is a relationship between fault splays and geothermal gradient variability. The outcomes of this study will further our understanding of geothermal resource distribution in the BMG. This understanding can be applied to other active extensional terranes with major graben structures, such as the Basins and Range province in southwestern USA and will provide guidance for future geothermal energy investigation and development.
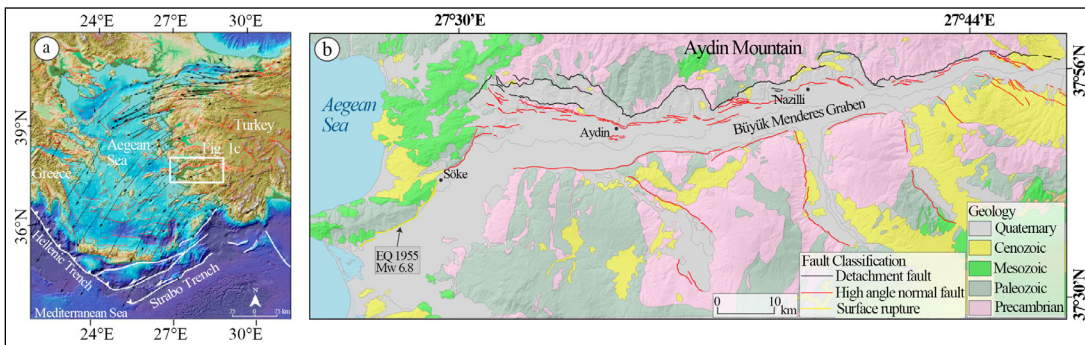
Figure 1- Western Anatolia maps showing the geology and relief of the BMG (Özpolat et al., 2020). a) Simplified active tectonic map of Western Anatolia and the Aegean Sea. b) Geological map of Aydın Mountain and the BMG.
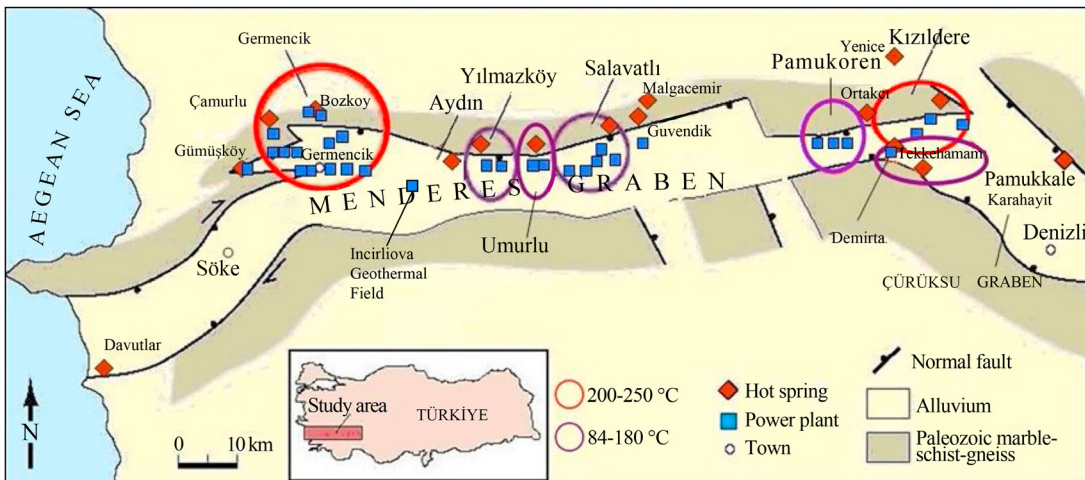
Figure 2- Map of power plants and hot springs in BMG (Modified from Faulds et al., 2010; Yamanlar et al., 2020). Temperatures indicated by circles represent the reservoir temperature range for each system.
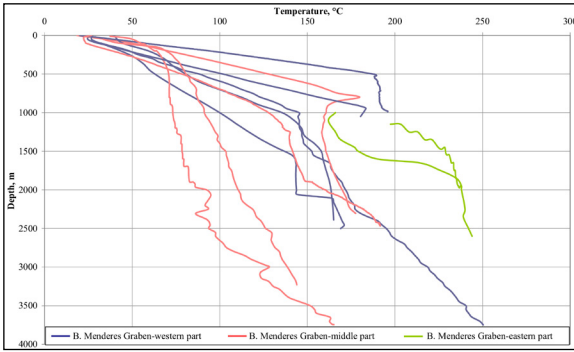
Figure 3- Geothermal gradients in the west, central, and eastern sections of the BMG (Yamanlar et al., 2020).

1.1. Statement of Problem

This study aims to use interpolation to model the 3D variation of geothermal gradient with respect to rock units present in the Incirliova Geothermal Field in the central section of the BMG and compare them to other models developed in different areas of the BMG.

The main objectives of this study are:

- To identify the regions of high temperature in the subsurface in the Incirliova Geothermal Field area within the BMG based on the interpretation of available well logs together with temperature logs;

- To develop a 3D model for the stratigraphy and temperature distribution of the Incirliova Geothermal Field;

- To develop isothermal contour maps at 50°C intervals for the Incirliova Geothermal Field area;

- To compare the 3D temperature model created using bottom hole temperatures with one that includes continuous temperature logs; and

- To compare the 3D temperature model of a centrally located Incirliova Geothermal Field to those in the western and the eastern parts of the BMG.

1.2. Methodology

We used well temperature measurements, well logs, and heat flow data with 3D modeling software to create spatial models of the BMG with respect to lithology and temperature. HD Energy Solutions acquired a variety of data for thirteen different geothermal wells from the Incirliova Geothermal Field (IGF) (Figure 4). Twelve of the wells included BHT information and were used for this study. Eleven of those wells
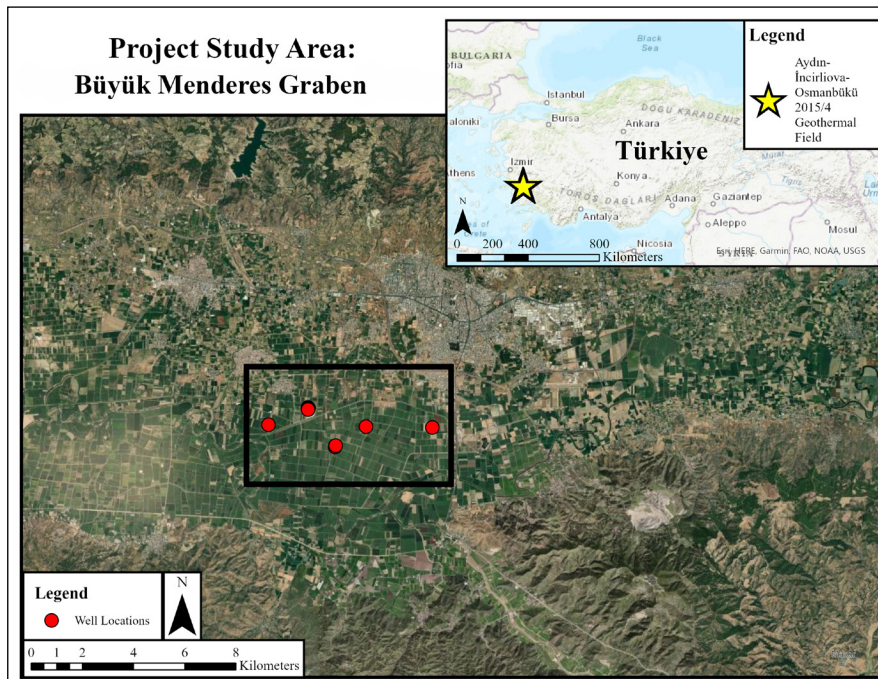
Figure 4- Location of study area and wells. The top right inset map shows the location of the BMG in Türkiye. The larger bottom map shows the generalized location of the IGF and thirteen wells used in this study. Some of the wells were drilled from the same platform, making their locations, provided in overlap on the map.

included stratigraphic columns. The twelve wells used in modeling are the following: Incirliova 1, Incirliova 2, Incirliova 3, Incirliova 4, Incirliova 5, Incirliova 6, Efeler-1, Batı Efeler-1, Incirliova Enjeksiyon-1, Incirliova Enjeksiyon-2, Incirliova Enjeksiyon-4, and Incirliova Enjeksiyon-5.

Seequent Leapfrog Geothermal software (Leapfrog) is used to develop the 3D models using the well data. The lithologic logs from the wells provided stratigraphic control for the geologic modeling. Temperature logs were used in addition to BHT to create a combined temperature model. These efforts estimated the basin geometry and stratigraphy within the IGF and the spatial temperature distribution in two different scenarios. The geometry, stratigraphy, and temperature distribution were then compared with other geothermal fields from the east and west sections of the BMG.

2. Main Text

2.1. Geologic Overview

2.1.1. Tectonic Evolution

The Western Anatolia Extended Terrane (WAET) is one of the best-developed examples of post-collisional extended terranes worldwide. It WAET, which includes BMG, is bounded by the North Anatolian Fault Zone to the north, by the Lycian nappes to the south and by the ENE-trending Southwest Anatolian Shear Zone (SWASZ) to the southeast.

Çemen et al. (2006) suggested that in the Cenozoic Era, Western Anatolia, Turkey experienced three consecutive stages of northward extension (Figure 5). Before the Cenozoic extension occurred, the Menderes massif formed from several events. First, the Pan African orogeny in Cambro-Ordovician time formed the core metamorphic rocks, then the Alpine orogeny from Mesozoic through Cenozoic time formed the overlying sequence of metamorphic rocks (Çemen et al., 2006). The first stage of the extension was initiated by orogenic collapse around 30 Ma in Late Oligocene time (Figure 5a and b). This extension initiated the SWASZ and the Gokova, Kale, and Tavas basins. During the second extension stage, beginning in the Early Miocene time, the Alaşehir and Büyük

Menderes Grabens were formed (Figure 5c), likely due to the subduction roll-back of the Aegean subduction zone (Cemen et al., 2006). Geochronology using argon dating also suggests subduction roll-back has occurred in the WAET throughout the Miocene (Uzel et al., 2020). The third stage of the extension was initiated about 5 Ma ago in Late Miocene to the Early Pliocene time, when the westward escape of the Anatolian Plate started, and generated high angle oblique-slip normal faults in the graben (Figure 5d). Based on gravity modeling, Alemdar (2015) and Mahatsente et al. (2017) have suggested that the asthenospheric material has risen through the lithosphere up to the mantle-crust interface beneath the BMG at 29°E (Figure 5). Recent studies have suggested that the BMG evolved from a supra-detachment basin in the Miocene to a rift basin in the Pliocene and Quaternary using a rolling-hinge model for basin evolution (Sümer et al., 2020).

2.1.2. Stratigraphy

Three main rock groups in the BMG (Figure 7) are the Pre-Neogene basement rocks, Neogene sedimentary units, and Quaternary deposits (Sert, 2015). The basement rocks are high-grade metamorphic rocks such as marble, gneiss, and schist (Cemen et al., 2006). The sedimentary rock units include three successions that unconformably overly each other (Cohen et al., 1995; Bozkurt, 2000; Göğüş, 2004; Şen and Seyitoğlu, 2009): the Early-Middle Miocene Başçayır, the Late Miocene Aydın, and the Pliocene Huseyinciler formations (Sert, 2015; Merey, 2016). Unconformably overlying these sedimentary rock formations is the Quaternary Hamzali Formation (Kazancı et al., 2009).

Pre-Neogene Metamorphic Basement Rocks

The Pre-Neogene metamorphic basement rocks of the BMG (Figure 7) consist of metamorphic rocks of the Menderes Metamorphic Core Complex (MMCC). These rocks were exhumed due to extensional tectonics in the region (Seyitoğlu et al., 2002; Çemen et al., 2006; Gessner et al., 2013). It is suggested that the fractures in these metamorphic rocks provide the heat exchange necessary to achieve the high temperatures observed in the region (Faulds et al., 2010). Roche et al. (2019) suggested that some marble is karst, which provides pockets of geothermal fluids.
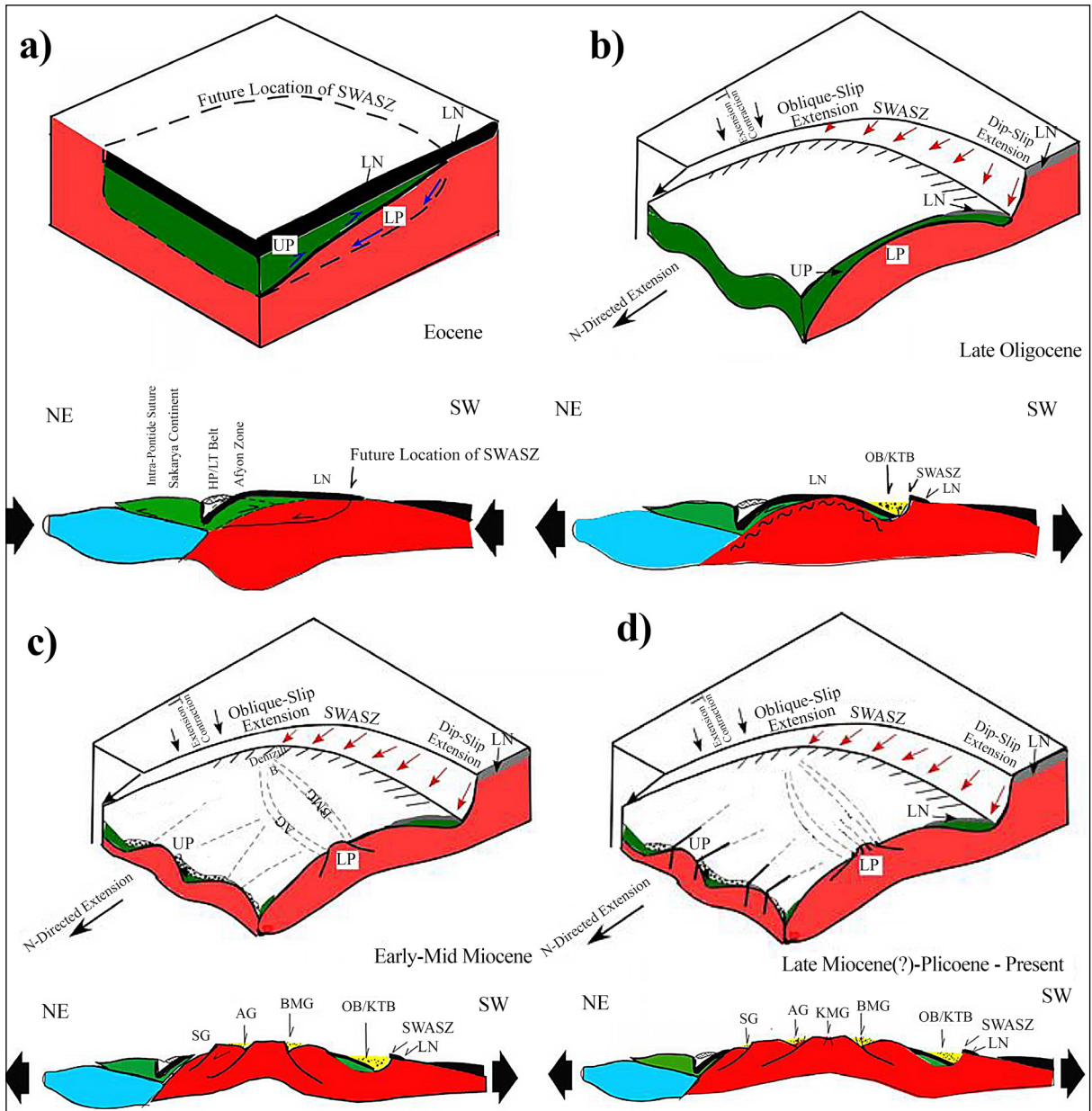
Figure 5- 3D cartoons and related schematic cross-sections (modified from Seyitoğlu et al., 2004; Sert, 2015) displaying the proposed three-stage extensional model of the Cenozoic evolution of Western Türkiye in a) Eocene, b) Late Oligocene, c) Early to Middle- Miocene and d) Late Miocene-Pliocene to present (not to scale). Abbreviations: AG: Alaşehir Graben; BMG: Büyük Menderes Graben; OB/KTB: Ören and Kale-Tavas basins; KMG: Kucuk Menderes Graben; LN: Lycian nappes; LP: lower plate; SG: Simav graben; SWASZ: Southwest Anatolian shear zone; UP: upper plate (from Çemen et al., 2006).

Başçayır Formation

The Başçayır Formation is the oldest syn-extensional sedimentary sequence (early-middle Miocene) in the BMG (Çifçi et al., 2011). There is an unconformable boundary between the Başçayır Formation and the metamorphic basement rocks. The base of the unit is conglomerate and overlain by a shale-dominated sequence that is laterally filled with alluvial fan deposits (Cohen et al., 1995).

Aydın Formation

The Aydın Formation (late Miocene) consists of a coarse-grained conglomerate with interbedded layers of sandstone, mudstone, and claystone (Bozkurt,
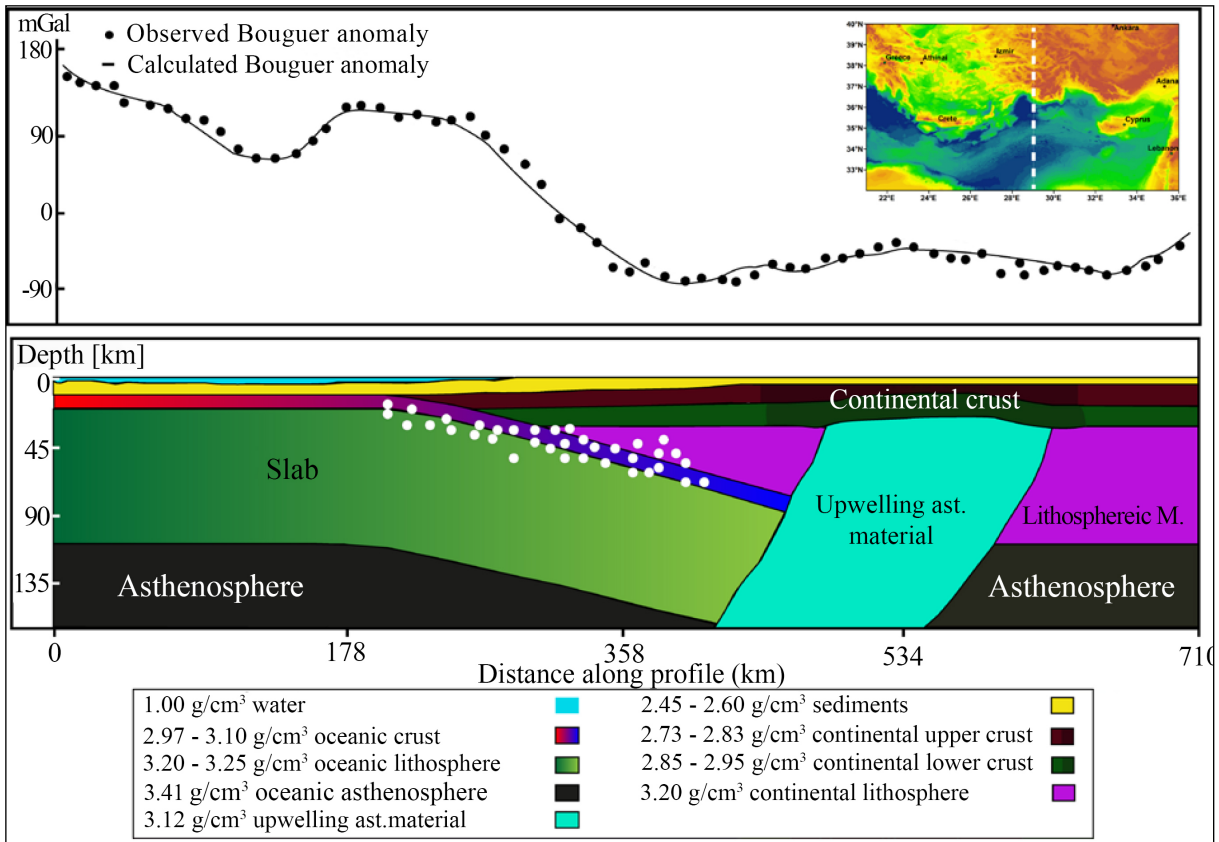
Figure 6- 2.5-D gravity model along a north-south transect at 29°E (Alemdar, 2015; Mahatsente et al., 2017). The upwelling asthenospheric material is underneath the BMG.

2000; Şen and Seyitoğlu, 2009). The clastic sediments in this formation were sourced from the Menderes Metamorphic Core Complex rocks and the rocks of the underlying Başçayır formation. The Aydın Formation was also deposited syn-extensionally (Sert, 2015). Sert, 2015, interpreted N-S oriented seismic reflection cross sections of the BMG and showed that the Aydın Formation is thicker in the center and gradually thinner towards the north and south edges. This is also evident in the cross section (Figure 10) published by Lovekin et al. 2019.

Hüseyinciler Formiation

The Huseyinciler Formation (Pliocene) consists of alluvial and fluvial clastic rocks, namely poorly-sorted conglomerates in a clay matrix with interbedded sandstone and mudstone (Yılmaz et al., 2000).

Quaternary Alluvium (Hamzalı Formation)

The Quaternary Hamzalı Formation consists of alluvial fan deposits and modern clastic sediments commonly found along the northern boundary of the BMG. The Büyük Menderes River carries the clastic sediments from east to west in the BMG. This succession is thicker in the east and mostly consists of mud and muddy sand (Kazancı et al., 2009; Çiftçi and Bozkurt, 2010).

2.1.3. Structural Geology

The BMG is the largest active graben in Western Anatolia. It has been proposed that the BMG formed by normal faulting along the main graben bounding fault, the Büyük Menderes Detachment, that is south-dipping and located along the northern side of the graben (Çemen et al., 2006; Şen and Seyitoğlu, 2009). The modern Büyük Menderes Detachment is low-angle, but kinematic evolution studies suggest it originally formed at a high angle (Merey, 2016). Continuous motion along the detachment is suggested to be responsible for the thicker syn-depositional sequences found in the center of the graben, which thin towards the north and south (Yılmaz et al., 2000;

Era	Period	Epoch	Formation	Thickness	LITHOLOGY	DESCRIPTION
CENOZOIC	QUATERNARY		Hamzali	(250 m)		Gravel, sand, silt and clay
	NEOGENE	Pliocene	Huseyinciler	(350 m)		Conglomerate, sandstone, and mudstone
		Late Miocene	Aydin	(1200 m)		Conglomerate, sandstone, siltstone, marl, mudstone, claystone, and clayey limestone
		Early-Middle Miocene	Bascayir	(600 m)		Boulder, conglomerate, sandstone, siltstone, mudstone, and limestone
PALAEOZOIC-MESOZOIC			Menderes Metamorphics			Basement rocks: Gneiss, schist, and marble
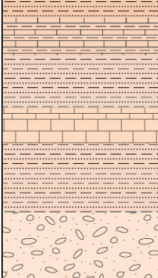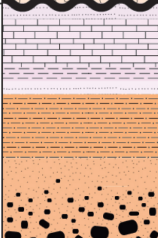
Figure 7- Generalized stratigraphy of the BMG (modified from Sert, 2015).

Seyitoğlu et al., 2004; Çemen et al., 2006; Sen and Seyitoğlu, 2009; Sert, 2015).

The low-angle graben detachment faults, initiated during the second stage of extension (Figure 5c), and high-angle normal faults, initiated during the third stage (Figure 5d), intersect at the interface between the Başçayır Formation and the basement rocks. It was previously thought that the BMG exhibited a rollover structure similar to that of the Alaşehir Graben north of the BMG (Seyitoğlu et al., 2004). Merey (2016) proposed new evidence suggesting that the BMG does not contain a rollover structure and was instead formed by active rifting. However, the origin of rifting remains to be not well understood.

Roche et al. (2019) performed a structural analysis of two geothermal fields in the BMG: the Germencik field in the west and the Salavatlı geothermal field in the east. Both of these geothermal fields are along the northern flank of the graben, near the main detachment fault. Faulds et al. (2009) analyzed the structure of the Germecik, Aydın, Yılmazköy, and the Kızıldere geothermal fields, and realized that they are found all along the northern detachment fault of the graben.

Faulds et al. (2010) suggested that within the Germencik geothermal field, horsetailing fault terminations exist in the basement rock (Figure 8), creating highly porous and permeable fractured rock that serves as reservoirs for geothermal fluids. The high surface areas of these reservoirs also allow high rates of heat transfer between the rock and the fluids. The faults then act as conduits for the fluids to return to the surface, where they may be utilized for geothermal energy production.

2.1.4. Heat Flow in the BMG

Roche et al. (2019) examined both a local-scale and basin-scale analysis of the geothermal activity in the BMG with respect to structural, lithological, and geodynamic controls. Based on oxygen, hydrogen, and helium isotopes studies of geothermal waters from the BMG, it has been suggested that the heat source of the BMG is not of magmatic origin (Roche et al., 2019). Instead, the source of heat in the BMG is shallow asthenospheric material at the interface with the crust. Geophysical surveys, including kinematic reconstruction and gravity surveys of the subsurface, also have suggested that there is a slab tear beneath the eastern portion of the BMG, which results in uplifting asthenosphere to the east (Figure 5) (Alemdar, 2015; Merey, 2016; Mahatsente et al., 2017).

2.1.5. Geothermal Fields in the BMG

Conventional geothermal systems require a source of high temperatures, reservoirs (permeable and porous lithology) with large quantities of hot fluids, a cap rock (impermeable lithology) above the reservoir, and a permeable pathway for fluid recharge (Roche et al., 2019). These conditions are all present in many areas in the BMG, which explains its geothermal potential and its numerous geothermal fields that are actively producing renewable clean energy. As of 2019, there were 27 operating geothermal fields in Western Anatolia, and 16 of those were in the BMG (Mertoğlu et al., 2019). Tonkul et al. (2021) conducted a case study of the Germencik Geothermal Field in the western BMG. They used numerical modeling to create a 3D distribution of the subsurface temperatures in the field (Figure 8). This study aims to similarly model a different geothermal field that corresponds to "Aydın-Incirliova Field" in Mertoğlu et al. (2019). This field will hereby be known as the Incirliova Geothermal Field (IGF).

2.1.6. Incirliova Geothermal Field

The IGF is ~7 km SE from the town of Incirliova, and ~7 km SW from the city of Aydın, and ~15 km SE from the Germencik Geothermal Field. The production, exploration and injection wells in this field are arranged in an overall E-W trend (Figure 4). The IGF is about halfway between the north and south margins of the BMG (Figures 1 and 9), which locates it in the western-central part of the graben, and far from the surface outcropping of either of the

detachment faults of the BMG. The reservoir target of the drilling program was a fractured marble formation in the metamorphic basement (Lovekin et al., 2019). The IGF was developed by the company 3S Kale. A published seismic reflection profile of the field (Figure 10) shows that the northern faults dip southward and the southern faults dip northward (Lovekin et al., 2019), which is consistent with the interpretations of other reflection seismic profiles in the graben (Sert, 2015; Merey, 2016).
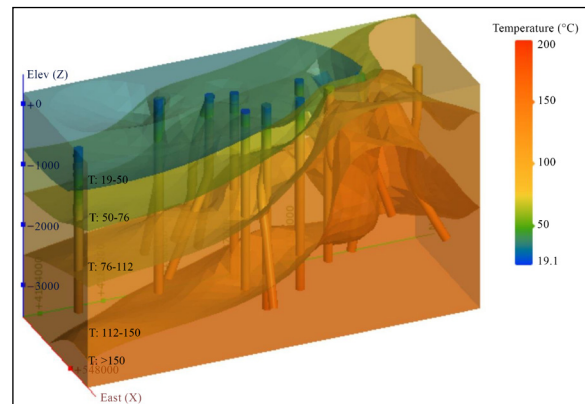
Figure 8- Numerical 3D temperature model of the Germencik Geothermal Field, facing SW (Tonkul et al., 2021).

2.2. Data

Data from thirteen geothermal wells drilled in Incirliova Geothermal Field were supplied by HD Energy Solutions for this study. Data provided with the wells included the name of well, date, name of the quadrangle, well coordinates at wellhead, coordinates at the total depth, depth in MD and TVD, the temperature at kelly bushing and at total depth (BHT), maximum discharge, and state of the well (production or injection). In addition, wireline logs (temperature and pressure), mud loss, and lithology logs were supplied for eleven wells. One of the wells, Osmanbükü-1 did not have BHT information. The dates provided with both the BHT and well log data span between 2015 and 2018, before the plant began operating in late 2018. This suggests that both data sets could be exploration data and that the BHT and temperature logs could be combined within one model. This is uncertain, however, and the BHTs could be production data instead.
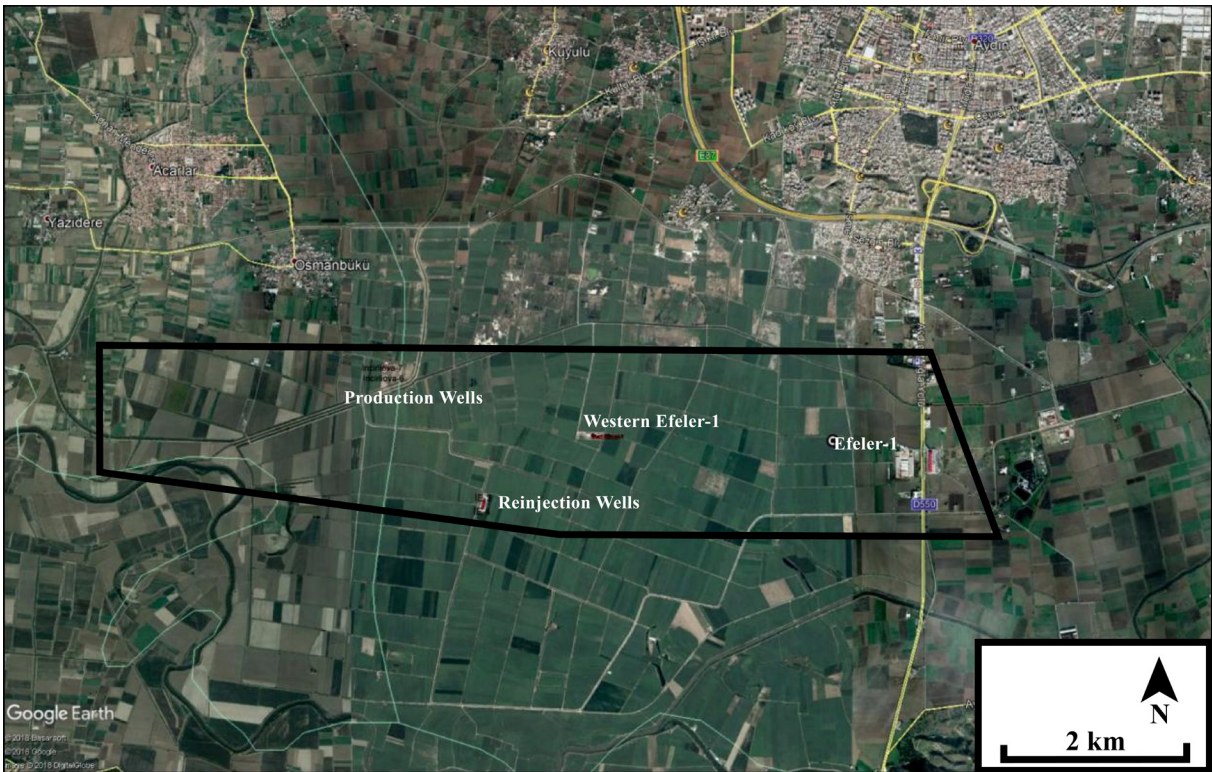
Figure 9- Location of the geothermal lease for the IGF (Modified from HD Energy Solutions).
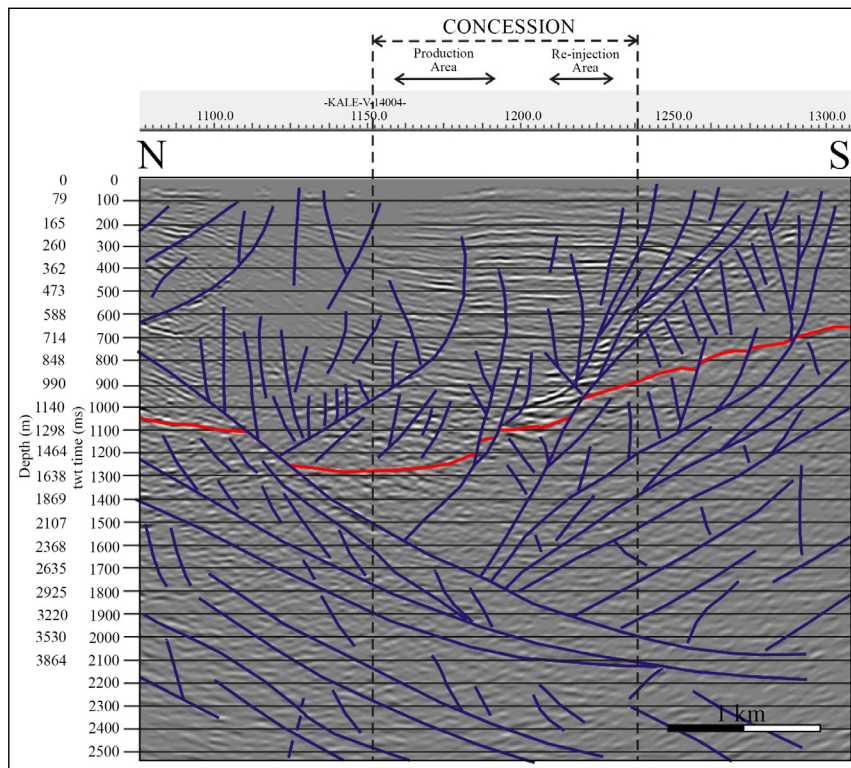
Figure 10- Seismic cross-section of the IGF, showing faults illustrated in the section. The red line represents the boundary between the Başçayır Formation and the basement metamorphics (Lovekin et al., 2019).

2.3. Modeling, Outputs, and Observations

The models generated for this study used Leapfrog Geothermal and ArcMap software. The wells were plotted in ArcMap to check their location. Once the locations of the wells were confirmed, the map was exported as a georeferenced image and imported into Leapfrog. The digital elevation model (DEM) data were constrained to a dataframe of the same size as the well location map and that was exported as raster images and imported into Leapfrog.

2.3.1. Well Deviation

The subsurface well data were prepared in file formats which were compatible with Leapfrog. This included converting XY coordinates of top and bottom of the well into spherical coordinates, so the 3D well deviation could be plotted in Leapfrog.

2.3.2. Temperature Data

The file formatting also included preparing the temperature data. To prepare the data for BHT interpolation, the average atmospheric surface temperature and the BHT were used. For each well, the average atmospheric temperature of the region, 18.2 °C, was assigned to the depth at 0 m, and the BHT was assigned as the temperature at total depth. The temperature logs were provided in graphical image format, so they first needed to be digitized into a numeric data set. To do so, the temperature logs were first upscaled to a higher resolution by tracing and redrawing in Adobe Illustrator. Then the online application Plot Digitizer was used to assign numeric values to the continuous data series for temperature.

2.3.3. Generating the Models

A workflow was derived to aid the completion of this study (Figure 11). Three models were prepared for the project once the files were loaded into Leapfrog. The geologic model was created first. It was constructed from youngest to oldest. This simultaneously preserves volume while honoring the boundaries of the model, the DEM, and the well data. Since no other independent geophysical data, such as 2D or 3D seismic lines, were available, the geologic models are not constrained by any additional information. The next two models were temperature models based on numeric modeling. The second model created was the BHT-driven temperature model. It was created using atmospheric surface temperature and BHT for each well, then interpolating the wells' temperatures in three dimensions. The third model used the five available continuous temperature logs and combined them with BHT data for any well without a temperature log. The interpolation method used to generate the numerical models was Radial Basis Function.
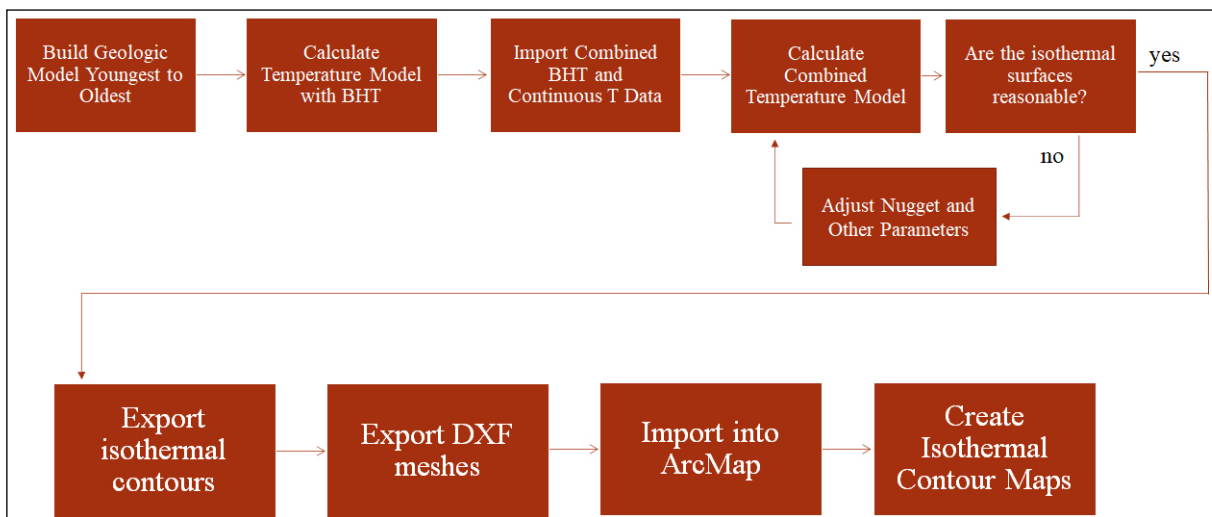
Figure 11- Modeling and contour map-making workflow.

2.3.4. Creating Isothermal Contour Maps

A combination of Leapfrog and ArcMap software was used to create the isothermal contour maps. Two main types of data were first exported from Leapfrog, then those files were used to construct the isothermal maps in ArcMap. First, the desired temperature model in Leapfrog was selected. Second, the "Isocontour" tab was selected and used to generate contour lines in shapefile format at 100 m intervals for the temperature isosurfaces in the model. Third, the same temperature isosurface was selected in Leapfrog and was used to export a mesh as a DXF file.

Fourth, a new project was started in ArcMap. The corresponding DXF file, and contour lines were imported for each isothermal contour map. The Spatial Analyst toolbox in ArcMap was used to create an elevation raster from the polyline mesh provided by the DXF file. The output raster was the subsurface elevation distribution at a given temperature. The raster was then assigned a reasonable color gradient to represent the depth distribution. Then, the isothermal contour lines were overlaid on the temperature and

formatted as contour lines using the properties panel within the data layer in ArcMap. This is followed by a final map, created using Layout View in ArcMap. The process was repeated for each isothermal contour used in each temperature model.

2.4. Model Outputs and Observations

Each model of the Incirliova Geothermal Field (IGF) is bounded by a rectangular prism with the following dimensions: 7190 m in length, 2084 m in width, and 4320 m in depth. The unit used for the scale in each figure is in meters (m). All figures are true-to-scale.

2.4.1. Geologic Model

The observed lithologies of the wells were used as constraints to determine the geologic model. The wells are shown as 3D cylinders with the color-coded lithology according to the formation list in the figure (Figure 12). As stated in the stratigraphy section, the geologic model (Figure 12) includes the basement metamorphic rocks and the overlying
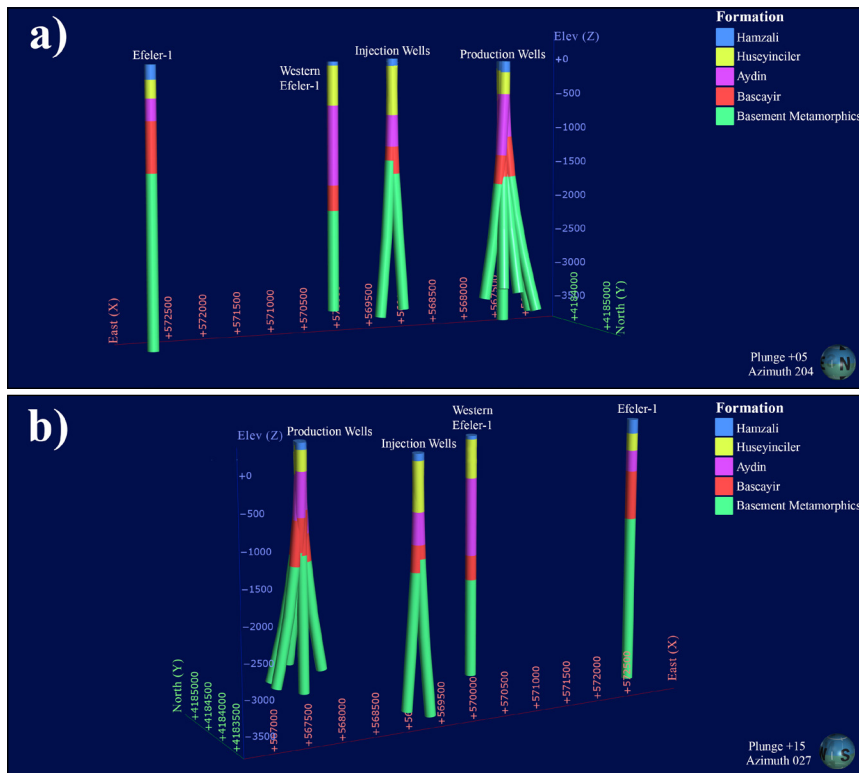
Figure 12- a) Lithology of the wells facing SW, Names of wells are included, b) Lithology of the wells facing SE.

four main Cenozoic sedimentary rocks succession. The formation names honor the names provided in the stratigraphic column (Figure 7). It follows the stratigraphy of basement metamorphic rocks, followed by early-middle Miocene rocks (Başçayır Formation) late Miocene rocks (Aydın Formation), Pliocene rocks (Hüseyinciler Formation), and Quaternary sediments (Hamzalı Formation).

The 3D model output shows that the sedimentary rock formations are not of equal or consistent thickness. The Başçayır Formation, in red, shows thickest sediments in the northeast section of the field (Figure 13). Meanwhile, the Başçayır Formation appears to pinch-out in the southwest section of the field (Figure 14). In general the sedimentary rock formations appear thickest towards the north, where their location roughly represents the midway point between the north and south flanks of the BMG.

2.4.2. Temperature Models

The results of temperature modeling include both the 3D models generated in Seequent Leapfrog and the isothermal contour maps as described in section 3.2.4.

3D Temperature Models

The first temperature model generated for the geothermal field used only BHT and atmospheric temperature for each well (Figure 15 and 16). The temperatures in each well were interpolated in 3D across the field's subsurface within the constraints of the model.
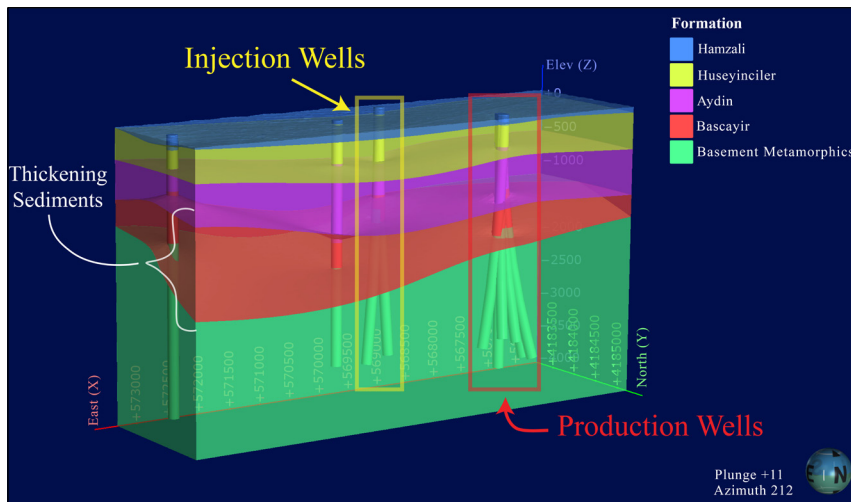
Figure 13- Overall 3D geologic model of the IGF, view is to the SW (azimuth 212°). The injection wells are outlined in yellow, and the production wells are outlined in red.
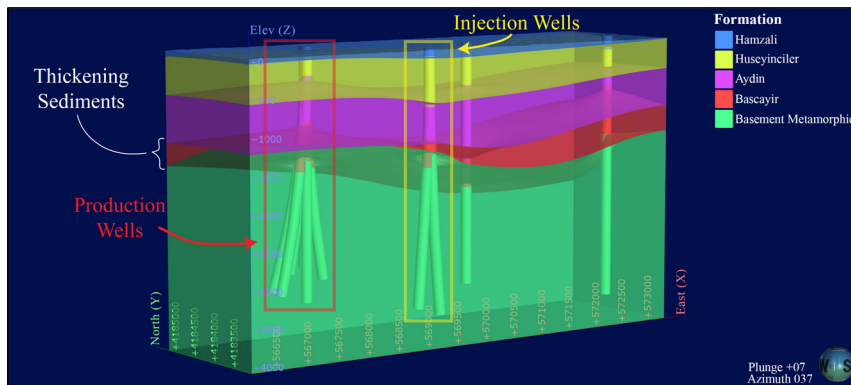
Figure 14- A 3D geologic model of the IGF, view is to the NE (azimuth 037°).
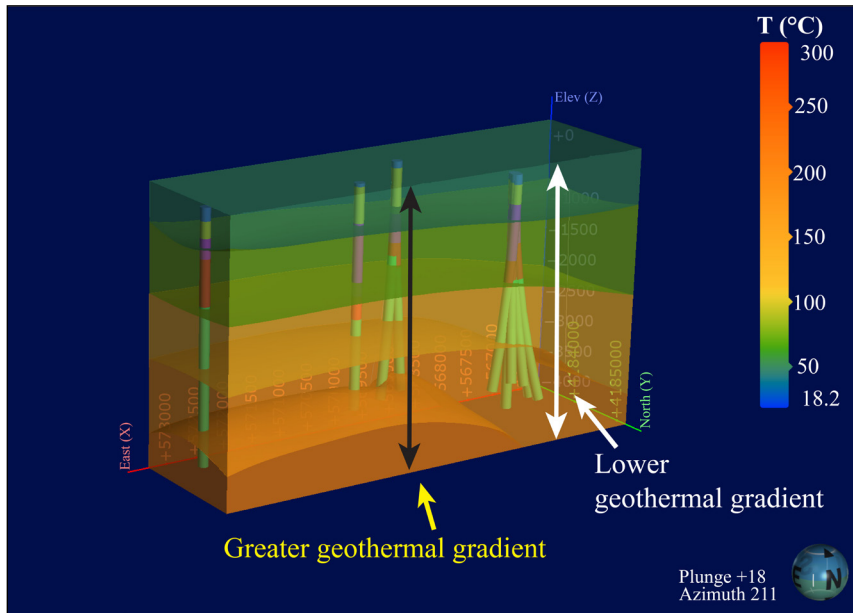
Figure 15- The 3D geothermal gradient based on BHT in the IGF, view to the SW (azimuth 211°). Isothermal contours at 50°C intervals are shown as surfaces of solid color.
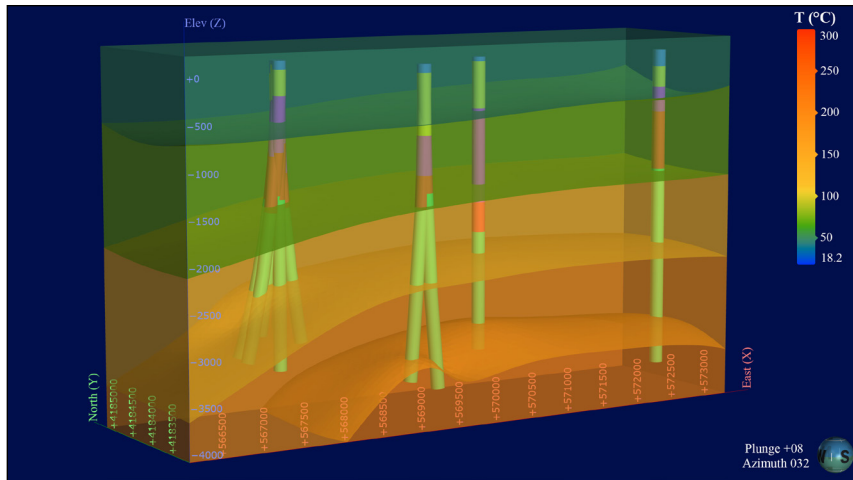
Figure 16 – BHT temperature model of the IGF, view is to the NE (azimuth 032°).

The second temperature model generated for the geothermal field combined all available continuous temperature logs with BHT data from the wells with no temperature logs. These temperatures were interpolated the same way as stated in the previous model.

2.4.3. Isothermal Contour Maps

The isothermal contour maps show the temperature isosurfaces from the 3D models as seen on a map view with contour lines. Each contour line is 100 m. Each map represents one temperature at 50°C intervals for each geothermal temperature model constructed in Leapfrog. Four maps were made for the BHT-driven model and five maps were made for the continuous temperature model (Figure 17). One example map from each set is shown for the 50°C contour (Figure 18 and 19).
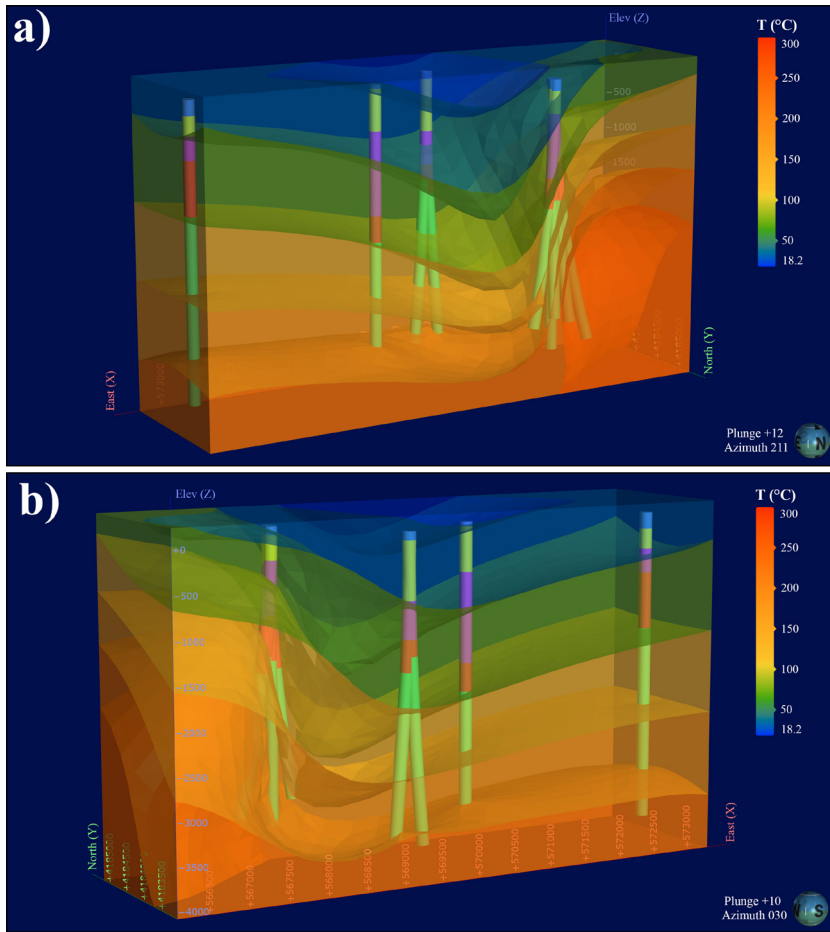
Figure 17- a) Temperature model combining BHT and continuous temperature data of IGF, view is to the SW (azimuth 211°), b) Temperature model combining BHT and continuous temperature data of IGF, view is to the NE (azimuth 030°).
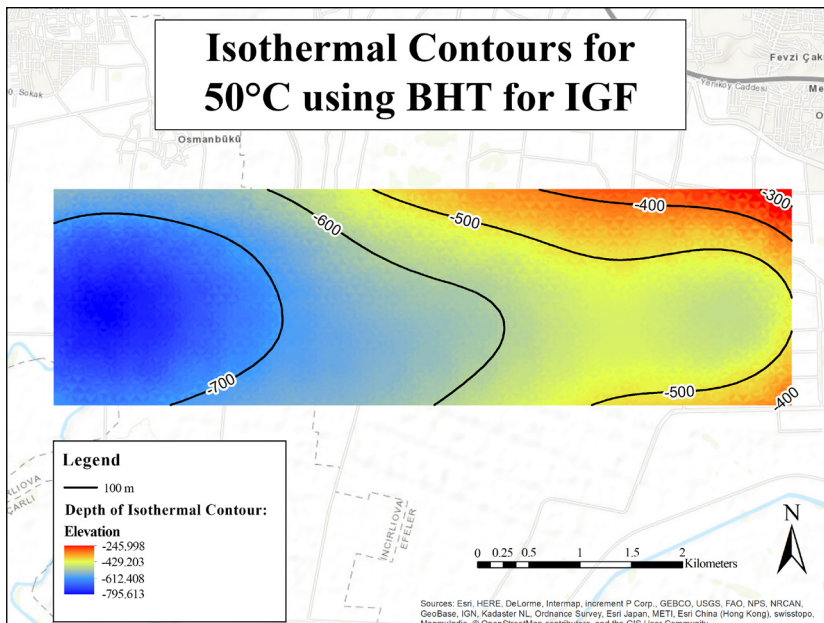
Figure 18- Example of isothermal contour map created for the IGF BHT model at 50°C.
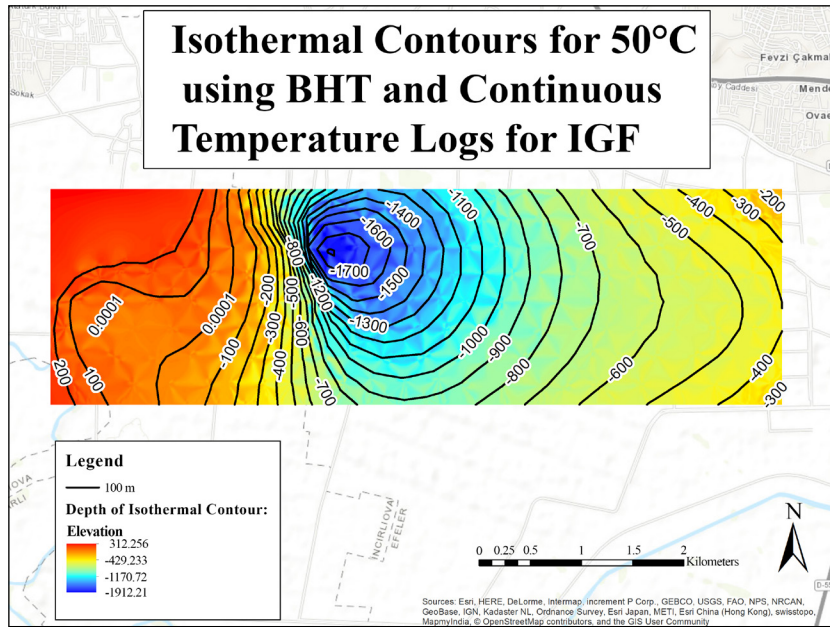
Figure 19- Example of isothermal contour map for isothermal contour map with continuous temperat ure logs.

3. Discussion

3.1 Discussion of Geologic Model

3.1.1. Implications for Geothermal Production

In the geologic model, the total depths of the wells penetrate the metamorphic basement rocks. This shows that the targeted reservoir formation in the IGF is the metamorphic basement. The basement rock most likely makes a better reservoir rock because it has high heat transfer capabilities. The top of the metamorphic basement likely contains erosional features and fractures which allow high surface area for heat transfer to geothermal fluids. Some of these fractures are observable as fault surfaces in the published cross-section from Lovekin et al. (2019) (Figure 10). Other important characteristics of the reservoir include the physical characteristics derived from its composition. Since the metamorphic basement reservoir contains marble, it is likely that some $CaCO_3$ has dissolved in the hot geothermal fluids and created voids in the subsurface. These features likely include interconnected spaces that can fill with geothermal fluids. The fractures, erosional features, and dissolution features all likely aid convective heat transfer by allowing higher permeability, porosity, and, subsequently, flow of geothermal fluids within and along the top of the basement.

3.1.2. Implications for Sedimentation and Tectonics

On the southern side of the geologic model, the Başçayır Formation appears to "pinch out" and the basement rocks and the late Miocene rocks form a contact (Figure 13 and 14). It is unlikely that the Başçayır Formation is absent due to its original position or sedimentation. Instead, the absence of the Başçayır Formation is possibly due to normal faulting along a north dipping fault. This is also apparent in the thicknesses of the Başçayır Formation reported in the well logs and as seen in lithologic model (Figures 13 and 14). Furthermore, compared to the production wells, the Başçayır-Aydın contact occurs at greater depth in the injection wells. The Başçayır Formation is much thinner in one of the injection wells, Incirliova Enjeksiyon-4, and this could be accounted for by both faulting and synextensional sedimentation. The synextensional sedimentation interpreted from the varying thicknesses of sedimentary rocks from this model is consistent with observations from rock outcrops and interpretations of structural data in the BMG from other studies (Sümer et al., 2020).

The model suggests that synextensional sedimentation occurred in this region. When compared to the published seismic profile of Lovekin et al. (2019), the IGF is just south of the intersection of the

BMG's north and south graben bounding faults. Even without including fault surfaces in the model, the geologic model shows thicker sedimentary sections north of the production wells (Figure 13).

Fault surfaces were not included in this model because structural fault data was unavailable. If available, types of data that could be used to model fault surfaces could be surface structural measurements or seismic reflection data. 3D seismic reflection data would be optimal to model and interpret the fault surfaces in the subsurface. Despite the lack of fault modeling, the geologic model is still valid because the individual faults seen in the published cross-section from Lovekin et al. (2019) do not have much displacement (Figure 10).

Active sedimentation in basins is known to suppress heat flow within the basins (Theissen and Rüpke, 2010). The effect of active sedimentation in the BMG most likely suppresses heat flow, but it might not be consistently suppressed throughout the basin. Since the most sedimentation occurs in the center of the graben, it is likely that heat flow is most suppressed in the center of the graben and the least suppressed at the north and south boundaries where the sediment is thinnest.

3.2. Discussion of Temperature Models and Isothermal Contour Maps

3.2.1. Isothermal Contour Maps

Figures 18 and 19 use a map view to show the spatial distribution of the isothermal contours that were created in Leapfrog. Each map shows an isocontour surface that represents a single temperature. These surfaces are called isothermal contours, and, for each model, every map displays a different temperature value that increases sequentially by 50°C. The elevation where that temperature occurs in subsurface is represented by a color gradient and elevation contour lines. In the color gradient, blue represents greater depth and red represents closer proximity to the surface.

The first set of isothermal contour maps show the distribution of temperature based on the BHT-driven model (Figure 18). These maps show greater geothermal gradients in the east and lower geothermal

gradients in the west. The contours have a gentle slope to the west with a relative maximum in the eastern portion.

The second set of isothermal contour maps show the distribution of temperature based on the continuous temperature model (Figure 19). In general, these maps show greatest geothermal gradient in the west and lesser geothermal gradients in the eastern IGF. Due to modeling error, the very western portion of these maps may show unrealistic results of high temperatures close to the surface. The validity and handling of this discrepancy in results is further discussed in section 3.2.3. With respect to the maps, the error causes the color gradient for depth to be less helpful in interpreting subsurface temperatures for the 50, 100, and 150 °C isothermal contours in this map set. The isothermal contour lines are still accurate for the surfaces generated in the modeling. The slight rise in slope to the west may not be reasonable, but the steep slopes, as seen by many contour lines stacked on top of each other, show a steep uplift of temperature that is observed in the 3D models. This section is where the production wells are drilled, as observed in Figures 15 and 16.

3.2.2. Implications for Reservoir Management and Data Source

In the BHT temperature model, the greatest geothermal gradient is at the site of the injection wells, and the lowest geothermal gradient is at the site of the production wells (Figure 15). While this seems counter-intuitive, it could be explained based on the data source. If the BHT data used in this study was from a well-monitoring service sometime after production was initiated, then the geothermal system may have reached thermal equilibrium, which has resulted in the phenomenon known as "thermal breakthrough." This refers to a condition in the field that occurs after production begins. In this scenario, during sustained production, the subsurface temperatures of the reservoir at the production wells decrease over time until the system reaches equilibrium.

In the combined temperature model, the subsurface temperatures at the production wells are elevated, and significant 250°C temperature isosurfaces are visible (Figure 17). Compared to the BHT temperature model, the 200°C thermal isosurface in the combined model

occurs 2000 m closer to the surface. This difference in the depth suggests a thermal breakthrough has occurred in the reservoir. The elevated temperatures are shown for all the temperature isosurfaces in the western portion of the IGF. However, the temperatures in the east side of the IGF appears relatively consistent when the two models are compared. This may be due to the BHT data used to supplement the continuous temperature data. Overall, the elevated temperatures in the production region suggest that the continuous temperature data was from the exploration stage and predates any thermal breakthrough in the reservoir.

However, if the differences between the BHT and combined temperature models are not a result of geothermal production, then it could be explained by natural causes. Since the BMG is actively extending and known to be seismically active (Figure 1), then the changes in the reservoir temperature over time could be the result of changes in the fracture and fault connectivity in the subsurface. Earthquakes in the region could cause new fractures and faults that allow new recharge and circulation patterns to form in the reservoir. For example, if colder recharge fluids were no longer able to enter the reservoir due to sealing by a fault, then the reservoir temperature might increase. In another hypothetical situation, colder geothermal fluids may be allowed to access the reservoir through newly formed fracture pathways, subsequently resulting in lower temperature distribution for the reservoir.

3.2.3. Comparison with the Germencik Geothermal Field (GGF)

The IGF is ~15 km SE of the GGF. The numerical temperature models of the IGF (Figure 15 and 16) from this study are compared to those of the GGF (Figure 8). In all the models, depths of up to about 3000 m are used. The combined temperature model from this study, and the GGF show similar uplifts of isothermal contours on one side of the geothermal field. Some of the isothermal contours may seem unreasonable in both the IGF combined model and the GGF model. This is because they extend to the surface, showing temperatures of 50 to 100°C extending to the surface, which is unrealistic. The unrealistic elevations of the isothermal contours can also be seen in the western parts of the isothermal contour maps (Figure 19). Nevertheless, the IGF and GGF models both show similar shapes of relatively high temperatures upwelling at depth into similar shapes. The IGF model shows similar temperatures at same depth as the GGF model, however the IGF model shows a 250°C contour around 2 km depth that the GGF model does not include. This suggests that the IGF has a higher geothermal gradient than the GGF at a depth of 2 km. The GGF case study by Tonkul et al. (2021) used 3D interpolative numerical modeling in Leapfrog to validate their reservoir temperature calculations obtained by geothermometry. In the GGF, geothermometry has shown that the reservoir temperature is between 190°C and 232°C (Tonkul et al., 2021). The reservoir temperatures for the GGF obtained by geothermometer calculations are consistent with those obtained by numerical modeling. Since the IGF models presented in this study closely resemble those of the GGF, which is validated by reservoir temperatures calculated by geothermometry, then it stands to reason that the IGF interpolative temperature models are valid.

3.2.4 Geothermal Gradient Variability throughout the BMG

The variability of the geothermal gradient throughout the BMG cannot be fully explained by this study. This study, however, does provide more insight to the factors which cause the variability. Regions of the BMG that feature highly fractured basement rock likely provide localized areas of higher geothermal gradients. The western portion of the BMG appears consistent with the interpretation that highly fractured basement rock creates conditions appropriate for high geothermal gradients. However, the eastern portion of the graben was not able to be evaluated in this study because data were not available from geothermal fields in the eastern BMG. Therefore, this study does not adequately test the hypothesis suggesting that the origin of high geothermal gradients and high heat flow in eastern portion of the graben is due to rising asthenospheric material. This hypothesis remains untested.

The distribution of temperature in the BMG is likely controlled by the distribution of convective hydrothermal systems throughout the region. Convective hydrothermal systems require adequate

permeability for heat and fluid flow to occur. Structural geologic setting has been identified as the main control of permeability distribution in extensional settings (Faulds et al., 2010). The IGF is unique in the fact that it is the only commercial geothermal system occurring greater than ~5 km from the surface expression of the Büyük Menderes Detachment. One possible structural setting for the IGF could be an intersection at depth between the northwest-striking Çine Graben fault, the Büyük Menderes Detachment, and the southern detachment fault. This structural intersection could provide enough permeability to create a commercial convective geothermal system occurring in the center of the BMG.

4. Results

The geologic models show a simplified structure within the BMG due to the omission of fault surfaces. Despite this, the geologic model is valid without fault surfaces because the individual faults do not have much displacement. Pinch-outs are observed in early versions of the model, which may be data-driven due to wells drilled on either side of a hydraulically conductive fault. The pinch-outs also may be error-introduced artifacts of software functions such as interpolation. However, the thicknesses of geologic units observed in the model show thicker sediments toward the center of the BMG, which suggests that synextensional deposition occurred in the graben.

The two temperature models, one made from bottom hole temperature (BHT) measurements and the other made from both continuous temperature logs and BHT data, suggest that the geothermal reservoir has experienced a thermal breakthrough, where reservoir temperatures at the production wells have declined over time via sustained production.

The IGF, a west-central geothermal field within the BMG, has similar characteristics to the GGF, a western-located geothermal field in the BMG. The IGF appears to have a higher geothermal gradient, as evident in the higher temperature isothermal contour surfaces shown at similar depths. This is likely due to a different structural setting involving the NW-striking Çine Graben fault; however, this hypothesis remains to be tested.

4.1. Recommendations

The spatial variability of the geothermal gradient in the BMG could be further described if more isothermal contour maps and 3D models, such as those created in this study, were created for other geothermal fields in the BMG. To fully explain the variability, other information would be needed to support the case. This information could include the fracture structures of the basement and sedimentary rocks and the behavior of the asthenosphere-lithosphere interactions.

The geologic models created in this study may be improved by using seismic reflection data and structural measurements to evaluate and include the effects of faulting within the geologic model.

With fault information included, numeric flow simulations, such as TOUGH2, could be combined with the Leapfrog models to create reservoir heat and fluid flow simulations. Other physical modeling software could be used, too. The physical models would improve the understanding of the temperature and heat flow distribution because they would be able to include more physical parameters and solve for equilibrium states of the subsurface. This would provide a more realistic estimation of the subsurface interactions between rocks, fluids, energy, and structural geology. The conductive heat flow of the IGF could be solved analytically by combining thermal conductivity values of rocks in Western Anatolia (Balkan et al., 2017) with the geologic model calculated in this study. The thermal conductivity values reported were for common rock types of Western Anatolia in both saturated and dry conditions. For geothermal systems, the saturated condition is used.

References

Alemdar, S. 2015. A model of the crust and upper mantle structure of the Hellenic and Cyprus subduction zones constrained by gravity and seismic data [M.S.]: The University of Alabama, 100 p., http://search.proquest.com/pqdtglobal/docview/1764970978/abstract/C59EED0D12424A60PQ/1 (accessed November 2020).

Balkan, E., Erkan, K., Şalk, M. 2017. Thermal conductivity of major rock types in western and central Anatolia regions, Turkey: Journal of Geophysics and Engineering, 14, 909–919.

Bozkurt, E. 2000. Timing of Extension on the Büyük Menderes Graben, Western Turkey, and Its Tectonic Implications: Geological Society, London, Special Publications, 173, 385–403.

Çemen, I., Catlos, E., Göğüş, O., Özerdem, C. 2006. Postcollisional Extensional Tectonics and Exhumation of the Menderes Massif in the Western Anatolia Extended Terrane, Turkey. In: Post-collisional Tectonics and Magmatism in the Eastern Mediterranean Region: Special Paper of the Geological Society of America, 409, 353–379.

Çiftçi, N. B., Bozkurt, E. 2010. Structural evolution of the Gediz Graben, SW Turkey: temporal and spatial variation of the graben basin: Basin Research, 22, 846–873.

Çifçi, G., Pamukçu, O., Çoruh, C., Çopur, S., Sözbilir, H. 2011. Shallow and Deep Structure of a Supradetachment Basin Based on Geological, Conventional Deep Seismic Reflection Sections and Gravity Data in the Buyuk Menderes Graben, Western Anatolia: Surveys in Geophysics, 32, 271–290.

Cohen, H. A., Dart, C. J., Akyüz, H. S., Barka, A. 1995. Syn-rift sedimentation and structural development of the Gediz and Büyük Menderes graben, western Turkey: Journal of the Geological Society, 152, 629–638.

Faulds, J., Bouchot, V., Moeck, I., Oğuz, K. 2009. Structural controls of geothermal systems in western Turkey: A preliminary report: Geotherm Resou Counc Trans, 33, 375–383.

Faulds, J., Coolbaugh, M., Bouchot, V., Moek, I., Oğuz, K. 2010. Characterizing Structural Controls of Geothermal Reservoirs in the Great Basin, USA, and Western Turkey: Developing Successful Exploration Strategies in Extended Terranes, in p., https://hal-brgm.archives-ouvertes.fr/hal-00495884 (accessed November 2020).

Gessner, K., Gallardo, L.A., Markwitz, V., Ring, U., Thomson, S. N. 2013. What caused the denudation of the Menderes Massif: Review of crustal evolution, lithosphere structure, and dynamic topography in southwest Turkey: Gondwana Research, 24, 243–274.

Göğüş, O. H. 2004. Geometry and Tectonic Significance of Buyuk Menderes Detachment, in the Bascayir Area, Buyuk Menderes Graben, Western Turkey:, https://shareok.org/handle/11244/8019 (accessed December 2020).

Haklıdır, F. S. T., Şengün, R. 2020. Hydrogeochemical similarities and differences between high temperature geothermal systems with similar geologic settings in the Büyük Menderes and Gediz Grabens of Turkey: Geothermics, 83.

Kazancı, N., Dündar, S., Alçiçek, M. C., Gürbüz, A. 2009. Quaternary deposits of the Büyük Menderes Graben in western Anatolia, Turkey: Implications for river capture and the longest Holocene estuary in the Aegean Sea: Marine Geology, 264, 165–176.

Lovekin, J., Görür, N., Şile, H. 2019. Case Study of the 3S Kale Incirliova Geothermal Project, Aydın Province, Turkey: 43, 6.

Mahatsente, R., Alemdar, S., Çemen, I. 2017. Effect of Slab-Tear on crustal structure in Southwestern Anatolia: Insight from Gravity Data Modelling: Geophysical Monograph Series.

Merey, O. 2016. Kinematic evolution of the Büyük Menderes Graben in western Turkey inferred from 2-D seismic interpretation and cross section restoration [M.S.]: The University of Alabama, 117, http://search.proquest.com/pqdtglobal/docview/1877637004/abstract/EB02A76D8A4286PQ/1 (accessed November 2020).

Mertoğlu, O., Şimşek, Ş., Başarır, N., Paksoy, H. 2019. Geothermal Energy Use, Country Update for Turkey:

Özgür, N., Çalışkan, T. A. 2013. Active Geothermal Systems in the Menderes Massif, Western Anatolia, Turkey: Procedia Earth and Planetary Science, 7, 652–655.

Özpolat, E., Yıldırım, C., Görüm, T. 2020. The Quaternary landforms of the Büyük Menderes Graben System: the southern Menderes Massif, western Anatolia, Turkey: Journal of Maps, 16, 405–419.

Roche, V., Bouchot, V., Beccaletto, L., Jolivet, L., Guillou-Frottier, L., Tuduri, J., Bozkurt, E. 2019. Structural, lithological, and geodynamic controls on geothermal activity in the Menderes geothermal Province (Western Anatolia, Turkey): International Journal of Earth Sciences, 301.

Şen, S., Seyitoğlu, G. 2009. Magnetostratigraphy of early–middle Miocene deposits from east–west trending Alaşehir and Büyük Menderes grabens in western Turkey, and its tectonic implications.

Sert, S. 2015. Subsurface structural geology of the eastern part of the Büyük Menderes Graben, western Turkey. [electronic resource] : implications for structural evolution of the Büyük Menderes and Alasehir Grabens: [University of Alabama Libraries].

Seyitoğlu, G., Işık, V., Çemen, I. 2004. Complete Tertiary exhumation history of the Menderes Massif, western Turkey: an alternative working hypothesis: Terra Nova, v. 16, p. 358–364.

Sümer, Ö., Sözbilir, H., Uzel, B. 2020. Evolving from Supra-Detachment to Rift Basin in Rolling Hinge Model of the Büyük Menderes Graben: Türkiye Jeoloji Bülteni-Geological Bulletin of Turkey, 63.

Theissen, S., Rüpke, L. H. 2010. Feedbacks of sedimentation on crustal heat flow: New insights from the Vøring Basin, Norwegian Sea: Basin Research, 22, 976–990.

Tonkul, S., Baba, A., Demir, M. M., Regenspurg, S. 2021. Characterization of Sb scaling and fluids in saline geothermal power plants: A case study for Germencik Region (Büyük Menderes Graben, Turkey): Geothermics, 96, 102227.

Uzel, B., Kuiper, K., Sözbilir, H., Kaymakçı, N., Langereis, C. G., and Boehm, K. 2020. Miocene geochronology and stratigraphy of western Anatolia: Insights from new Ar/Ar dataset: LITHOS, 352–353.

Yamanlar, S., Korkmaz, E. D., Serpen, Ü. 2020. Assessment of geothermal power potential in Buyuk Menderes Basin, Turkey: Geothermics, 88.

Yılmaz, Y., Genç, Ş. C., Gürer, F., Bozcu, M., Yılmaz, K., Karacık, Z., Altunkaynak, Ş., Elmas, A. 2000. When Did the Western Anatolian Grabens Begin to Develop? Geological Society, London, Special Publications,173, 353–384.